NJC

Accepted Manuscript

This is an *Accepted Manuscript*, which has been through the Royal Society of Chemistry peer review process and has been accepted for publication.

Accepted Manuscripts are published online shortly after acceptance, before technical editing, formatting and proof reading. Using this free service, authors can make their results available to the community, in citable form, before we publish the edited article. We will replace this *Accepted Manuscript* with the edited and formatted *Advance Article* as soon as it is available.

You can find more information about *Accepted Manuscripts* in the Information for Authors.

Please note that technical editing may introduce minor changes to the text and/or graphics, which may alter content. The journal's standard Terms & Conditions and the Ethical guidelines still apply. In no event shall the Royal Society of Chemistry be held responsible for any errors or omissions in this *Accepted Manuscript* or any consequences arising from the use of any information it contains.

ROYAL SOCIETY OF CHEMISTRY

www.rsc.org/njc

Journal Name

RSCPublishing

ARTICLE

Microwave-Assisted Synthesis of Bovine Serum Albumin-Gold Nanoclusters and Their Fluorescence-Quenched Sensing of Hg^{2+} ions

Cite this: DOI: 10.1039/xoxxoooooox

Received ooth January 2012,
Accepted ooth January 2012

DOI: 10.1039/xoxxoooooox

www.rsc.org/

Nai-Yue Hsu and Yang-Wei Lin*

This study presents the microwave-assisted synthesis of fluorescent bovine serum albumin (BSA)-gold (Au) nanoclusters (NCs). The as-prepared BSA–Au NCs exhibit red fluorescence (λ_{em} = 650 nm), large Stoke shift (300 nm), and high quantum yield (1.9%). Transmission electron microscopy revealed the BSA-Au NCs to be well dispersed, with an average diameter of 2.1 ± 0.3 nm. By conducting energy dispersive x-ray spectroscopy, X-ray photoelectron spectroscopy, fluorescence anisotropy analysis, Raman spectrometry, and matrix-assisted laser desorption mass spectrometry, we confirmed that metallic the Au NCs were successfully embedded in the BSA. Because of the metallophilic properties of Hg^{2+} ions and Au^{+} ions, the degree of interaction between the ions induced fluorescence quenching, and thus the change in fluorescence at 650 nm was dependent on the Hg^{2+} ion concentration. Under optimal conditions (0.1 × BSA-Au NCs; 5.0 mM 4-(2-hydroxyethyl)-1-piperazineethanesulfonic acid buffer at pH 7.0), the limit of detection for Hg^{2+} ions at a signal-to-noise ratio of 3 was 2.98 nM. We used this nanosensor to determine Hg^{2+} concentration in environmental water samples (pond and seawater). This approach is advantageous because it is facile, accurate, and precise (the relative standard deviation of the three runs of each sample was less than 3%).

Introduction

Because Hg^{2+} ions have severe effects on human health and the environment, monitoring their levels in aquatic ecosystems is essential.[1-5] The United States Environmental Protection Agency (US EPA) has set the maximum level of mercury in drinking water to be 10 nM (2.0 ppb).[6, 7] Inductively coupled plasma mass spectrometry (ICPMS) and X-ray fluorescence spectrometry are powerful techniques for determining ultra-trace amounts of Hg^{2+} ions in environmental and biological samples.[8-10] However, the aforementioned techniques are expensive and thus unsuitable for the on-site analysis of water samples. Therefore, developing sensitive, selective, and reliable analytical techniques for determining Hg^{2+} ion concentration is crucial.

Fluorescent gold (Au) nanoparticles (NPs) are often known as Au nanoclusters (NCs).[11, 12] Au NCs comprise few to several tens of Au atoms. They have attracted considerable attention because they provide molecule-like behavior, thus linking atoms and NPs.[11] Au NCs exhibit size-dependent fluorescence properties because their sizes are comparable with the Fermi wavelength of an electron. Fluorescent Au NCs are advantageous because of their favorable water solubility, low toxicity, remarkable photophysical properties, and facile surface modification, thus making them suitable for use in applications such as biosensors, molecular imaging, and nanolabeling.[13, 14] Various protein-based synthesis approaches to preparing fluorescent Au NCs are attracting increasing attention.[15, 16] When proteins are used for preparing fluorescent Au NCs, chemical reductants are not required. During preparation, proteins first coordinate with Au^{3+} through cysteine and histidine residues, which act as templates. The tyrosine residue of the protein under basic conditions (pH > 10.0) has been considered as favoring the reduction of Au^{3+} ions to Au^{0} atoms. This means that proteins act as reducing and stabilizing agents. Because the as-prepared Au NCs possess favorable photophysical properties, such as a long fluorescence lifetime (>20 ns), large Stokes shift (>100 nm), and high quantum yield, they can be used to develop sensitive fluorescent sensors. For example, Xie et al. first demonstrated a simple method for preparing fluorescent bovine serum albumin (BSA)-Au NCs.[12] The prepared Au NCs comprised 25 Au atoms, which exhibited red fluorescence.[11] The BSA-Au NC surface was stabilized using a small amount of Au^{+} ions, which have high affinity for metallophilic interaction with Hg^{2+} ions. This resulted in the effective quenching of the fluorescence of the BSA-Au NCs, which exhibited a remarkably high

sensitivity for Hg^{2+} ions, with a limit of detection (LOD) as low as 0.5 nM. Hu et al. prepared Au NCs in the presence of BSA, and these Au NCs have been used for detecting Hg^{2+} ions with an LOD of 80 nM.[17] The sensing mechanism is based on photoinduced electron transfer (photoluminescence quenching). High temperatures have been reported as favoring the formation of BSA-Au NCs. BSA-Au NCs prepared at 70 °C are sensitive to Hg^{2+} ions because of the metallophilic interaction between Au^{+} and Hg^{2+} ions. Such sensors could be used to detect Hg^{2+} ions with concentrations of 10–250 nM and an LOD of 4.0 nM.[18] Although Au NCs are sensitive and selective for detecting Hg^{2+} ions, they require a long preparation time. Microwave (MW)-assisted synthesis of BSA-stabilized Au NCs have attracted considerable attention because it provides uniform heating and requires a short reaction time.[19-24] The reaction time can be reduced from tens of hours to several minutes. The prepared Au NCs display strong red emission, which is quenched by nitrogen oxides, and thus Au NCs have great potential for determining the intracellular concentration of nitrogen oxides.[21] Wu et al. demonstrated a one-step MW-assisted method for synthesizing Au_{16}NCs@BSA and understanding the fluorescence-enhanced sensing of Ag^{+} ions.[22, 25] However, expensive microwave synthesis instruments are required.

In this study, MW-assisted synthesis of fluorescent BSA-Au NCs was demonstrated, and their fluorescence-quenching sensing of Hg^{2+} in environmental water samples was performed. The highlight of this study was that red light-emitting BSA-Au NCs were synthesized using a domestic MW oven (120 W) for 2 min. The parameters of the MW-assisted synthetic conditions, including the applied MW program, BSA concentration, and pH, are discussed in this paper. Ultraviolet (UV)-visible (vis) spectroscopy, fluorescence anisotropy spectroscopy, fluorescence spectroscopy, transmission electron microscopy (TEM), energy dispersive X-ray spectroscopy (EDS), Raman spectrometry, X-ray photoelectron spectroscopy (XPS), and matrix-assisted laser desorption mass spectrometry (MALDI-MS) were used to characterize the as-synthesized BSA-Au NCs. This paper concludes by exploring the potential of using BSA-Au NCs for determining Hg^{2+} concentration in environmental water samples.

Experimental sections

Chemicals

All chemicals used were of analytical grade or of the highest purity that was available. Hydrogen tetrachloroaurate (III) trihydrate ($HAuCl_4 \cdot 3H_2O$), BSA, human serum albumin (HSA), trypsin, lysozyme, sodium borohydride ($NaBH_4$, 98%), NaOH, 4-(2-hydroxyethyl)-1-piperazineethanesulfonic acid (HEPES), quinine sulfate, H_2SO_4, $AgNO_3$, $Pb(NO_3)_2$, $Ni(NO_3)_2 \cdot 6H_2O$, NaCl, $CaCl_2 \cdot 2H_2O$, $Sr(NO_3)_2$, $BaCl_2 \cdot 6H_2O$, $Cd(NO_3)_2 \cdot 4H_2O$, $FeCl_2 \cdot 4H_2O$, $Mg(NO_3)_2 \cdot 6H_2O$, $FeCl_3$, $HgCl_2$, $Co(NO_3)_2 \cdot 6H_2O$, $Cu(NO_3)_2 \cdot 2.5H_2O$, and KCl were obtained from Sigma Aldrich (St. Louis, MO, USA). 2,6-Pyridinedicarboxylic acid (PDCA) was purchased from Acros Organic (Jhonghe City, New Taipei City, TW). HEPES (0.05 M) buffer solutions were adjusted to pH 7.0 by using 2.0 M NaOH. Deionized water (18.2 MΩ·cm) was used to prepare all aqueous solutions.

Synthesis of BSA-Au NCs

In the MW-assisted synthesis, 5.0 mL of 65 mg/mL BSA was added to 5.0 mL of 10 mM $HAuCl_4 \cdot 3H_2O$, followed by 1.0 mL of 1.0 M NaOH. The mixture solution was heated with temporary pauses by using a domestic MW oven (120 W) for 2 min. The color of the solution turned from light yellow to orange-red. Under UV illumination, the solution exhibited red fluorescence, indicating the formation of BSA-Au NCs. For simplicity, the concentration of the as-prepared BSA-Au NCs is presented as 1×.

Characterization of BSA-Au NCs

The UV-Vis absorption and fluorescence spectra of the BSA-Au NCs were recorded using a UV-Vis spectrometer (Evolution 200; Thermo Fisher, Waltham, MA, USA) and fluorescence spectrometer (Varian, CA, USA), respectively. TEM (JEOL-1200EX II, Tokyo, Japan) was used to measure the size of the BSA-Au NCs. EDS (Oxford Instruments, Abingdon, UK) was used to confirm the compositions of the prepared nanostructures. Fluorescence anisotropy and Raman spectra of the BSA-Au NCs were recorded at room temperature by using a Cary Eclipse fluorescence spectrophotometer (Varian, CA, USA) and a confocal micro-Raman system (Thermo Fisher, Waltham, MA, USA), respectively. Mass spectra were recorded using a Microflex MALDI-MS (Bruker Daltonics, Bremen, Germany) in the positive ionization mode. XPS was performed using a VG ESCA210 electron spectrometer (VG Scientific, West Sussex, UK).

General procedure for sensing Hg^{2+} ions.

The BSA-Au NCs were added to 5.0 mM HEPES buffer solutions (pH 7.0) containing Hg^{2+} ions (0–1.0 μM) and interfering metal ions (100.0 μM). The final concentration of the BSA-Au NCs was 0.1×. The mixtures were equilibrated for 2.5 min and then, in the absence and presence of metal ions, were subjected to TEM, EDS, and fluorescence measurements.

Results and discussion

Synthesis and characterization of BSA–Au NCs

Figure 1 demonstrates the MW-assisted synthesis procedure of BSA-Au NCs. To avoid damage to the BSA, ensue efficient absorption of the MW energy, and result in rapid MW heating, water was selected as the reaction medium because of its favorable dielectric constant and dielectric loss constant.[21] In this study, MW irradiation was temporarily paused to prevent the reaction mixture from overheating. Figure 1 displays the fluorescence spectra of the BSA-Au NCs synthesized using a 2 min MW procedure. BSA-Au NCs1 was synthesized through 1.0 min MW irradiation, 1.0 min pause, and 1.0 min MW

irradiation. BSA-Au NCs2 was synthesized by 40 sec MW irradiation, 1.0 min pause, 40 sec MW irradiation, 1.0 min pause, and 40 sec MW irradiation. The final temperatures of the BSA-Au NCs1 and BSA-Au NCs2 were 57.1 and 62.5 ℃, respectively. High reaction temperatures favor the formation of high-quality BSA-Au NCs. Thus, the BSA-Au NCs2 had higher emission intensity than did the BSA-Au NCs1. The temperature of the BSA-Au NCs3 synthesized through 40 sec MW irradiation, 1.0 min pause, 40 sec MW irradiation, 1.0 min pause, 40 sec MW irradiation, 1.0 min pause, and 40 sec MW irradiation is approximately 80 °C. At reaction temperatures higher than 75 °C, BSA is denatured and forms an insoluble gel, and thus the yield of fluorescent BSA-Au NCs was low for the BSA-Au NCs3. As such, the MW procedure used for preparing the BSA-Au NCs2 was selected for further investigation.

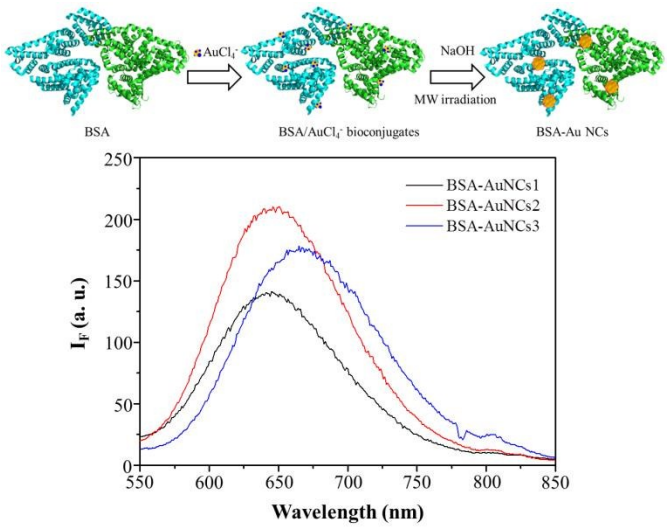

Figure 1. Schematic of the MW-assisted formation of BSA-Au NCs. Fluorescence spectra of BSA-Au NCs prepared using different MW irradiation procedures.

We investigated how BSA concentration and pH affected the formation of the BSA-Au NCs. As shown in Figure S1(a), the fluorescence intensity increased with an increase in the BSA concentration up to 32.5 mg/mL. A further increase in the BSA concentration resulted in nonuniform heating of the reaction mixture because of its viscosity caused by formation of BSA-Au NCs with low fluorescence intensity. Because pH affects protein structure, it is considered a crucial factor in the formation of BSA-Au NCs. The fluorescence intensity of the BSA-Au NCs increased with an increase in the pH from 9.0 to 11.0 (Figure S1(b)). This was mainly because of an increase in the reduction capability of the BSA. The tyrosine residue of BSA is responsible for reducing Au^{3+} to Au^{0} at pH levels greater than the pKa of tyrosine (approximately 10). At low pH levels (<10.0), the BSA did not exert a reducing effect on the formation of the BSA-Au NCs. At high pH levels (>11.0), a high NaOH concentration quenched the fluorescence intensity of the BSA-Au NCs.[26] In this study, the pH that resulted in the highest fluorescence intensity was 11.0.

At the optimal preparation conditions, the as-prepared BSA-Au NCs showed red emissions (λ_{em} = 650 nm) and a large Stoke shift (300 nm) (blue curve in Figure S2). The quantum yield of the as-prepared BSA-Au NCs was determined to be 1.9% by using a comparative method involving the use of quinine sulfate as a reference.[27] The BSA-Au NC solution increased absorbance between 300 and 400 nm (black curve in Figure S2), which was attributed to the formation of dityrosine residues in BSA and the nanoclusters.[28] The BSA-Au NCs did not show a surface plasmon resonance absorption band, demonstrating that large Au NPs with a diameter greater than 5 nm were not formed.[29, 30] Figure 2(a) displays the TEM images of BSA-Au NCs, indicating that the BSA-Au NCs were well dispersed, and that the average diameter was 2.1 ± 0.3 nm. Figure 2(b) and Figure 2(c) show the EDS and XPS spectra, respectively, of the BSA-Au NCs. The binding energies of Au $4f_{5/2}$ and Au $4f_{7/2}$ were 84.3 and 88.2 eV, respectively, for the as prepared BSA-Au NCs. Previous studies have reported the binding energies of Au $4f_{5/2}$ and Au $4f_{7/2}$ as being 83.9 and 87.7 eV, respectively, for the Au film.[27, 30] Thus, we expect that the surfaces of the BSA-Au NCs were covered by a small amount of Au^{+} ions.

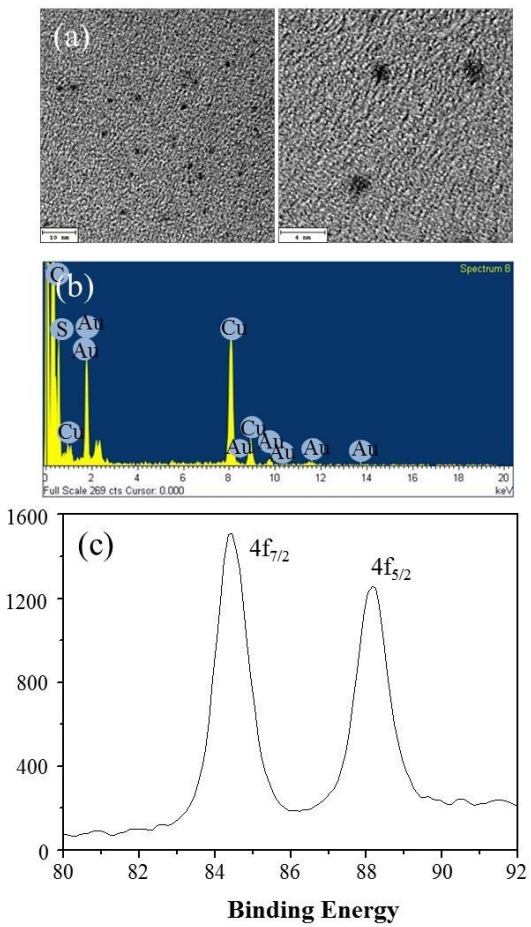

Figure 2. (a) TEM images, (b) EDS spectrum, and (c) XPS spectrum of BSA-Au NCs prepared under optimal conditions.

Fluorescence anisotropy, Raman spectroscopy, and MALDI-MS are useful for characterizing the protein templates

of Au nanomaterials. Figure S3(a) shows the recorded fluorescence anisotropy spectrum, indicating that the BSA-Au NCs had three decay times during the rotation transition (0.185, 3.84, and 43.2 ns). By using the Perrin equation, we calculated that the hydraulic radius of the BSA-Au NCs was 3.62 nm, which is close to the BSA gyration radius (3.48 nm).[31, 32] Figure S3(b) presents the Raman spectrum of the BSA-Au NCs, which is similar to that of free BSA.[33] In summary, we confirmed that metallic Au NCs were successfully embedded in the BSA. Figure S3(c) displays the MALDI-MS spectrum of the BSA-Au NCs. Two resolved peaks for BSA (*m/z* = 65.5 kDa) and BSA-Au NCs (*m/z* = approximately 69.4 kDa) were detected. The intensity of BSA is higher than that of BSA-Au NCs. These results indicated that only a small fraction of gold atoms/ions were released from BSA-Au NCs and subsequently redistributed to form BSA-Au_{20} NCs.[18] The atomic number of Au in this complex (20) coincides with the "magic numbers" of free Au_n clusters associated with the closing of the geometrical shells (*n* = 13, 20, 28, 38, and so on) or those of electronic shells (*n* = 8, 18, 20 34, and so on).[34, 35]

Sensing approach

Figure 3 shows that Hg^{2+} ion sensing based on the fluorescence quenching of BSA-Au NCs results from the metallophilic interaction between the Hg^{2+} and Au^{+} ions. Curve (a) in Figure 3 indicates the fluorescence spectrum of the BSA-Au NCs in 5.0 mM HEPES buffer solution (pH 7.0); the wavelength at maximal emission was 650 nm. We investigated how Hg^{2+} ions affect the fluorescence of the BSA-Au NCs in the HEPES buffer solution (5.0 mM, pH 7.0). As shown by curve (b) in Figure 3, the fluorescence quenching of the BSA-Au NCs occurred because of the d^{10}–d^{10} metallophilic interaction between Au^{+} ($4f^{14}5d^{10}$) and Hg^{2+} ($4f^{14}5d^{10}$) ions.[12] The TEM image displayed in Figure S4(a) shows that the size of the BSA-Au NCs in the presence of Hg^{2+} ions is the same as that in the absence of Hg^{2+} ions, indicating that Hg^{2+} ions had at most a slight effect on BSA-Au NC size. The EDS spectrum shows the Au and Hg peaks, thus proving the interaction between the Au^{+} and Hg^{2+} ions (Figure S4(b)).

Because $NaBH_4$ has a strong reductive ability to reduce Hg^{2+} to Hg^{0}, the interaction between Au^{+} and Hg^{2+} ions was destroyed. Thus, the addition of $NaBH_4$ apparently weakened the quenching effect of Hg^{2+} on BSA-Au NCs [curve (c) in Figure 3]. The recovered fluorescence intensity was slightly lower than that of free BSA-Au NCs. To elucidate how $NaBH_4$ affects BSA-Au, $NaBH_4$ was added to the BSA-Au NC solutions without Hg^{2+} ions. The fluorescence spectra of the BSA-Au NCs with $NaBH_4$ were the same in the absence and presence of Hg^{2+} ions, implying that $NaBH_4$ had at most a slight effect on the size of free BSA-Au NCs. The fluorescence images of the solutions in Figure 6 indicate that this probe allows the fluorescence detection of Hg^{2+} ions under UV illumination.

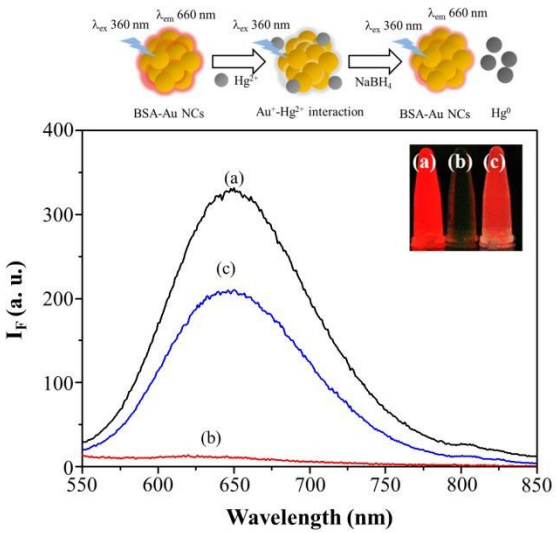

Figure 3. Schematic of Hg^{2+} sensing based on the fluorescence quenching of BSA-Au NCs that resulted from the metallophilic interaction between Hg^{2+} and Au^{+} ions. Fluorescence spectra of BSA-Au NCs (a) in the absence and (b) presence of Hg^{2+} ions (1.0 μM) and (c) in the presence of Hg^{2+} ions (1.0 μM) and $NaBH_4$ (1.0 M). The inset displays the images of BSA-Au NCs under the same conditions (λ_{ex}: 365 nm).

Sensing system optimization

Additional assay parameters were investigated to further optimize the experimental protocol. The fluorescence quenching of the BSA-Au NCs by the Hg^{2+} ions was measured as a function of time. As shown in Figure 4(a), the fluorescence intensity decreased rapidly following the addition of the Hg^{2+} ions. The intensity then decreased slightly with an increase in time from 0 to 150 sec and remained constant thereafter. Thus, we incubated the reaction mixture for 150 sec at room temperature in all assays.

The effect of BSA-Au NC concentration was investigated over the range 0.01–2.0×. Figure 4(b) shows the results of how BSA-Au NC concentration affected the values of $(I_{F0}–I_F)/I_{F0}$, where I_F and I_{F0} indicate that the fluorescence at 650 nm of BSA-Au NCs in the presence and absence of Hg^{2+} (1.0 μM), respectively. The $(I_{F0} - I_F)/I_{F0}$ value of the BSA-Au NCs increased with an increase in the BSA-Au NC concentration up to 0.1× and then slightly decreased, probably because of the inner filter effects of BSA-Au NCs at high concentrations. Therefore, 0.1× was selected as the optimal BSA-Au NC concentration.

The effect of pH for the HEPES buffer solution was investigated using a pH range of 6.0–8.0. As shown in Figure 4(c), the $(I_{F0} - I_F)/I_{F0}$ values for the BSA-Au NCs remained constant in the pH range of 6.0–8.0. Therefore, a HEPES buffer solution at pH 7.0 was used for all additional experiments. In addition, the effect of HEPES concentration on the system responses was investigated using 0.5–10 mM HEPES solutions (Figure 4(d)). The $(I_{F0} - I_F)/I_{F0}$ value increased slightly with an increase in the HEPES concentration up to 5.0 mM and then decreased. Therefore, 5.0 mM was selected as the optimal HEPES concentration.

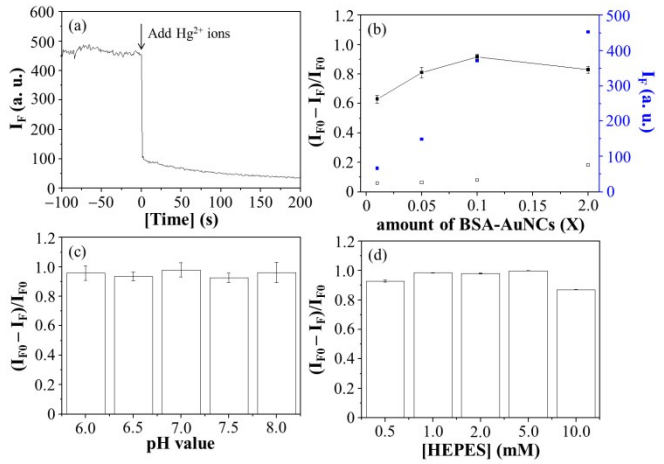

Figure 4. (a) Plot of time-dependent fluorescence intensity in the presence of Hg^{2+} ions (1.0 μM). $(I_{F0} - I_F)/I_{F0}$ values of the responses for various (b) BSA-Au NC concentrations, (c) pH values, and (d) concentrations of buffer solutions (HEPES buffer) for Hg^{2+} ion sensing. Error bars in the inset represent standard deviations from three repeated experiments.

Selectivity and sensitivity of the sensing system

To determine the selectivity of the BSA-Au NC probe toward Hg^{2+} ions, we conducted experiments similar to those used to obtain Figure 5. However, we added 100.0 μM of each of the following metal ions: Na^+, K^+, Ba^{2+}, Mg^{2+}, Ca^{2+}, Sr^{2+}, Cd^{2+}, Co^{2+}, Ni^{2+}, Pb^{2+}, Cu^{2+}, Ag^+, Fe^{3+}, and Fe^{2+}. Changes induced by the other metal ions were considerably smaller than those induced by 1.0 μM Hg^{2+} [$(I_{F0} - I_F)/I_{F0}$ = 0.95], except that of the Pb^{2+} ions (black bar in Figure 5(a)). This result showed that the fluorescence of the BSA-Au NCs was quenched through Pb^{2+}-mediated interparticle aggregation mechanism; free carboxylic groups of BSA on the particle surface easily interacted with Pb^{2+} ions.[36, 37] A greater selectivity of the BSA-Au NC probe of Hg^{2+} ions was readily achieved in the presence of the chelating ligand PDCA (1.0 mM).[38] PDCA forms considerably more stable complexes with heavy metal ions, such as Hg^{2+} (log β_2 = 20.28), than it does with other metal ions.[39, 40] To ensure favorable masking and the formation of stable complexes with Hg^{2+} ions, PDCA was added to each BSA-Au NC solution at a concentration of at least approximately 1000 times greater than that (1.0 μM) of Hg^{2+}. BSA-Au NCs in 5 mM HEPES buffer solution (pH 7.0) containing 1.0 mM PDCA responded selectively toward the Hg^{2+} ions by at least 10-fold more than they did for the other metal ions (red bar in Figure 5(a)). We suggest that some PDCA ligands bind to BSA-Au NC species through Au–N bonds, thus improving the selectivity of the probe toward Hg^{2+} ions through a cooperative effect.[39] PDCA ligands in bulk solutions formed complexes with other metal ions, suppressing their interference with the probe.

To further examine the practicality of using the probe, we conducted measurements in mixtures containing 1.0 μM Hg^{2+} and various potentially interfering ions (100.0 μM of Na^+, K^+, Ba^{2+}, Mg^{2+}, Ca^{2+}, Sr^{2+}, Cd^{2+}, Co^{2+}, Ni^{2+}, Pb^{2+}, Cu^{2+}, Ag^+, Fe^{3+}, and Fe^{2+}). The results suggested that most metal ions did not interfere with the determination of Hg^{2+}. The presence of other metal ions caused the values of the quenching effect induced by Hg^{2+} to vary by less than 0.05 units from the value obtained when only Hg^{2+} was present (Figure 5(b)).

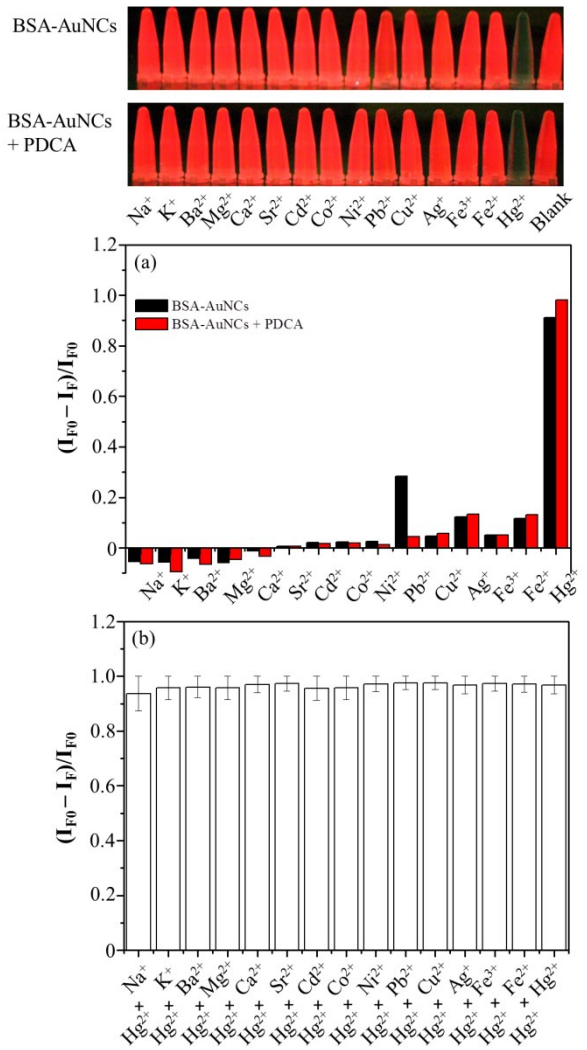

Figure 5. (a) Selectivities and (b) tolerances of the BSA-Au NCs probe for different metal ions (100 μM) and Hg^{2+} ions (1.0 μM) in 5.0 mM HEPES buffer (pH 7.0). Error bars represent standard deviations from three repeated experiments. Image shows the BSA-Au NC probes with different metal ions (λ_{ex}: 365 nm).

The fluorescence spectra of the BSA-Au NC solutions containing various Hg^{2+} concentrations, at optimized conditions, were recorded for use as a quantitative assay (Figure 6(a)). The fluorescence intensity of the BSA-Au NCs clearly decreased as Hg^{2+} concentration increased. A linear relationship was observed between the quenching effect and Hg^{2+} concentration in the concentration range of 5–100 nM, and the linear correlation coefficient was 0.933 (Figure 6(b)). The LOD for Hg^{2+}, defined as the concentration with a signal-to-noise ratio of 3, was 2.98 nM, suggesting that the probe is well suited for monitoring Hg^{2+} ions in environmental water samples, because

the highest Hg^{2+} concentration permitted by the US EPA in drinking water is 10 nM.

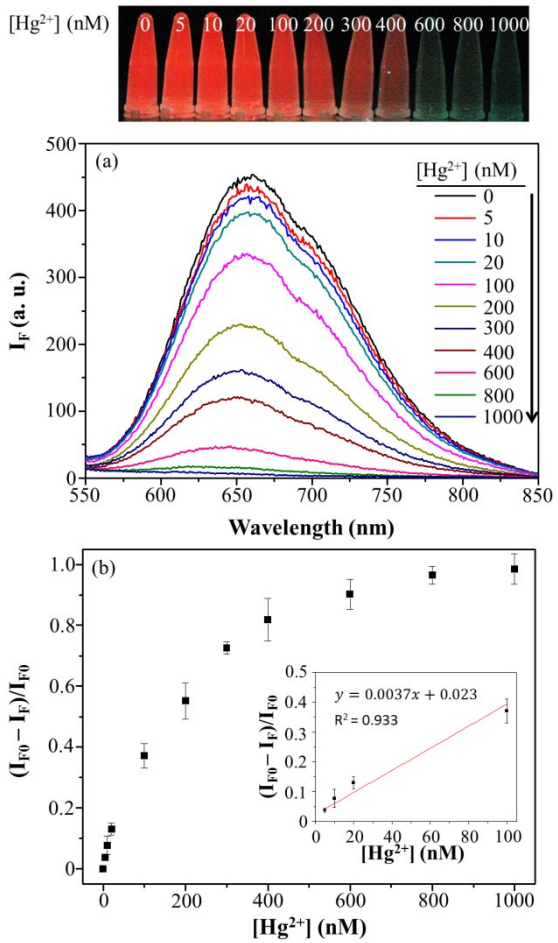

Figure 6. (a) Fluorescence spectra and (b) $(I_{F0} - I_F)/I_{F0}$ values for the responses of BSA-Au NCs for different Hg^{2+} ion concentrations. Inset: linear responses of the $(I_{F0} - I_F)/I_{F0}$ values plotted against Hg^{2+} ion concentrations. Error bars represent standard deviations from three repeated experiments. Image shows the BSA-Au NC probes with different Hg^{2+} ion concentrations (λ_{ex}: 365 nm).

Application in real samples

We expected the BSA-Au NC-based probe to exhibit great potential for use in analyzing Hg^{2+} in environmental water samples. We filtered water samples from a pond on our campus and from the coast in Taichung City, Taiwan, by using a 0.2 μm membrane, and subjected the filtrate to ICPMS analysis; no contamination of Hg^{2+} was determined. The trace Hg^{2+} ion concentrations in the pond and seawater were lower than the detection limit of our method (0.6 mL of water was added to 0.4 mL of 12.5 mM HEPES buffer solution containing BSA-Au NC probes). To demonstrate the feasibility of this approach for detecting Hg^{2+} ions in a complicated pond and seawater matrix, we applied a standard addition method to determine the Hg^{2+} ion concentration. A linear correlation was observed between the $(I_{F0} - I_F)/I_{F0}$ value and spiked Hg^{2+} concentration in each sample in the concentration range of 5.0–100 nM (Figure S5). The recoveries of these measurements were 97.7%–107%, and the LODs (for a signal-to-noise ratio of 3) for the Hg^{2+} in the pond and seawater matrix were 3.2 and 5.7 nM, respectively. We suggest that this probe will be useful for detecting environmentally relevant Hg^{2+} concentrations.

Conclusions

We prepared fluorescent BSA-Au NCs by using a domestic microwave oven for 2 min. To prevent overheating, the microwave irradiation was temporarily paused during the process. The MALDI-MS results showed that BSA-AuNCs consisted of 20 Au atoms. Fluorescence anisotropy and Raman data revealed that metallic Au NCs were successfully embedded in BSA. The fluorescent BSA-Au NCs were sensitive for detecting Hg^{2+} ions according to metallophilic Hg^{2+}-Au^{+} interactions, which effectively quenched the fluorescence of Au NCs. In addition, BSA-Au NCs possessed a great potential for detecting Hg^{2+} ions in pond and seawater samples. The use of this simple MW-assisted synthesis can be used to prepare HSA-, trypsin-, and lysozyme-stabilized Au NCs (Figure S6) and their applications for detecting antibodies and receptors are currently under way in our laboratory. This proposed method possesses several attractive features when compared with other reported methods (Table 1): (1) rapidity—it only takes 2 min to produce the highest fluorescence intensity of the BSA-Au NCs; (2) low cost and saving energy— a domestic microwave oven (120 W) can be used for the synthesis of BSA-Au NCs; (3) sensitivity—the LOD for Hg^{2+} ions is 2.98 nM; (4) practicality—analysis of complicated samples (pond, and seawater sample) is possible without performing tedious sample pretreatment; (5) extensive use—the proposed method can be used for the preparation of different kinds of protein-stabilized Au NCs.

Table 1 Protein-stabilized Au NCs-based on fluorescence quenched sensing of Hg^{2+} ions

Probe	Preparation method	Analytical range	LOD (nM)	Real sample	Ref.
BSA-Au NCs	37 ℃ / 12 hr	1–20 nM	0.5	-[a]	12
BSA-Au NCs	37 ℃ / 12 hr	0.4–43.2 μM	80	river, tap, mineral water	17
BSA-Au NCs	70 ℃ / 20 min	10–250 nM	4.0	pond water	18
Pepsin-Au NCs	37 ℃ / 2 hr	1–200 nM	1.0	-[a]	29
Lysozyme-Au NCs	37 ℃ / overnight	10 nM–5.0 μM	10	-[a]	30
Trypsin-Au NCs	37 ℃ / 24 hr	50–600 nM	50	river, tap, mineral water	41
AuNCs@BSA	MW[b] (37 ℃) / 2 hr	-[a]	0.6	-[a]	42
BSA-Au NCs	MW (120W) / 2 min	5–100 nM	2.98	pond, seawater	This study

[a]: not provided

[b]: CEM microwave (Discover SP model)

Acknowledgements

This study was supported by Ministry of Science and Technology under contracts (MOST 103-2113-M-018-001-

MY2). We thank Wallace Academic Editing for the English language editing.

Notes and references

Department of Chemistry, National Changhua University of Education,1, Jin-De Road, Changhua City, Taiwan; Tel: 011-886-4-7232105-3522
E-mail: linywjerry@cc.ncue.edu.tw

Electronic Supplementary Information (ESI) available: [Figure S1. Fluorescence intensities of BSA-Au NCs prepared using (a) various BSA concentrations and (b) pH.. Figure S2. Absorption spectra of BSA (red line) and BSA-Au NCs (black line). Fluorescence spectrum of BSA-Au NCs prepared under optimal conditions. Figure S3. (a) Fluorescence anisotropy, (b) Raman, and (c) MALDI-MS spectra of BSA-Au NCs. Figure S4. (a) TEM images and (b) EDS spectrum of BSA-Au NCs in the presence of Hg^{2+} ions. Figure S5. Standard addition analyses of (a) pond and (b) seawater samples examined using the BSA-Au NC probe. Figure S6. Fluorescence spectra of HSA-, trypsin-, and lysozyme-stabilized Au NCs.]. See DOI: 10.1039/b000000x/

1. A. A. Tinkov, O. P. Ajsuvakova, M. G. Skalnaya, E. V. Popova, A. I. Sinitskii, O. N. Nemereshina, E. R. Gatiatulina, A. A. Nikonorov and A. V. Skalny, *Biometals*, 2015, **28**, 231-254.
2. M. S. Gustin, H. M. Amos, J. Huang, M. B. Miller and K. Heidecorn, *Atmos. Chem. Phys.*, 2015, **15**, 5697-5713.
3. G. Q. Chen, Z. Guo, G. M. Zeng and L. Tang, *Analyst*, 2015, **140**, 5400-5443.
4. W. Chansuvarn, T. Tuntulani and A. Imyim, *Trac-Trend. Anal. Chem.*, 2015, **65**, 83-96.
5. A. Sharma, A. Sharma and R. K. Arya, *Sep. Sci. Technol.*, 2015, **50**, 1310-1320.
6. Y. W. Lin, C. C. Huang and H. T. Chang, *Analyst*, 2011, **136**, 863-871.
7. Y. W. Lin, C. W. Liu and H. T. Chang, *Talanta*, 2011, **84**, 324-329.
8. M. Noel, J. R. Christensen, J. Spence and C. T. Robbins, *Sci. Total Environ.*, 2015, **529**, 1-9.
9. M. P. Rodriguez-Reino, R. Rodriguez-Fernandez, E. Pena-Vazquez, R. Dominguez-Gonzalez, P. Bermejo-Barrera and A. Moreda-Pineiro, *J. Chromatogr. A*, 2015, **1391**, 9-17.
10. I. Rodriguez-Germade, B. Rubio and D. Rey, *Mar. Pollut. Bull.*, 2014, **86**, 458-467.
11. J. P. Xie, Y. G. Zheng and J. Y. Ying, *J. Am. Chem. Soc.*, 2009, **131**, 888-889.
12. J. P. Xie, Y. G. Zheng and J. Y. Ying, *Chem. Commun.*, 2010, **46**, 961-963.
13. F. Yan, X. Y. Liu, D. J. Zhao, W. X. Bao, X. P. Dong and F. N. Xi, *Prog. Chem.*, 2013, **25**, 799-808.
14. P. Yu, X. M. Wen, Y. R. Toh, X. Q. Ma and J. Tang, *Part. Part. Syst. Char.*, 2015, **32**, 142-163.
15. Y. H. Hu, W. J. Guo and H. Wei, *Isr. J. Chem.*, 2015, **55**, 682-697.
16. X. Yuan, X. Y. Dou, K. Y. Zheng and J. P. Xie, *Part. Part. Syst. Char.*, 2015, **32**, 613-629.
17. D. H. Hu, Z. H. Sheng, P. Gong, P. F. Zhang and L. T. Cai, *Analyst*, 2010, **135**, 1411-1416.
18. P. C. Chen, C. K. Chiang and H. T. Chang, *J. Nanopart. Res.*, 2013, **15**.
19. J. Zhang, Y. Yuan, Y. Wang, F. F. Sun, G. L. Liang, Z. Jiang and S. H. Yu, *Nano Res.*, 2015, **8**, 2329-2339.
20. L. Shang, L. X. Yang, F. Stockmar, R. Popescu, V. Trouillet, M. Bruns, D. Gerthsen and G. U. Nienhaus, *Nanoscale*, 2012, **4**, 4155-4160.
21. L. Yan, Y. Q. Cai, B. Z. Zheng, H. Y. Yuan, Y. Guo, D. Xiao and M. M. F. Choi, *J. Mater. Chem.*, 2012, **22**, 1000-1005.
22. Y. Yue, T. Y. Liu, H. W. Li, Z. Y. Liu and Y. Q. Wu, *Nanoscale*, 2012, **4**, 2251-2254.
23. D. H. Tian, Z. S. Qian, Y. S. Xia and C. Q. Zhu, *Langmuir*, 2012, **28**, 3945-3951.
24. D. F. He, Y. Xiang, X. Wang and X. F. Yu, *Mater. Res. Bull.*, 2011, **46**, 2418-2421.
25. H. W. Li, Y. Yue, T. Y. Liu, D. M. Li and Y. Q. Wu, *J. Phys. Chem. C*, 2013, **117**, 16159-16165.
26. J. P. Xie, J. Y. Lee, D. I. C. Wang and Y. P. Ting, *ACS Nano*, 2007, **1**, 429-439.
27. X. Le Guevel, B. Hotzer, G. Jung, K. Hollemeyer, V. Trouillet and M. Schneider, *J. Phys. Chem. C*, 2011, **115**, 10955-10963.
28. L. Su, T. Shu, J. X. Wang, Z. Y. Zhang and X. J. Zhang, *J. Phys. Chem. C*, 2015, **119**, 12065-12070.
29. H. Kawasaki, K. Hamaguchi, I. Osaka and R. Arakawa, *Adv. Funct. Mater.*, 2011, **21**, 3508-3515.
30. H. Wei, Z. D. Wang, L. M. Yang, S. L. Tian, C. J. Hou and Y. Lu, *Analyst*, 2010, **135**, 1406-1410.
31. S. Raut, R. Chib, R. Rich, D. Shumilov, Z. Gryczynski and I. Gryczynski, *Nanoscale*, 2013, **5**, 3441-3446.
32. E. Serefoglou, J. Oberdisse and G. Staikos, *Biomacromolecules*, 2007, **8**, 1195-1199.
33. C. C. Lin, Y. M. Yang, Y. F. Chen, T. S. Yang and H. C. Chang, *Biosens. Bioelectron.*, 2008, **24**, 178-183.
34. J. Li, X. Li, H.-J. Zhai and L.-S. Wang, *Science*, 2003, **299**, 864-867.
35. H. Häkkinen, R. Barnett and U. Landman, *Phys. Rev. Lett.*, 1999, **82**, 3264.
36. H. J. Zhu, T. Yu, H. D. Xu, K. Zhang, H. Jiang, Z. P. Zhang, Z. Y. Wang and S. H. Wang, *ACS Appl. Mater. Interfaces*, 2014, **6**, 21461-21467.
37. Z. Q. Yuan, M. H. Peng, Y. He and E. S. Yeung, *Chem. Commun.*, 2011, **47**, 11981-11983.
38. Y. Wang, F. Yang and X. R. Yang, *Biosens. Bioelectron.*, 2010, **25**, 1994-1998.
39. Y. W. Lin, W. T. Chen and H. T. Chang, *Rapid Commun. Mass Sp.*, 2010, **24**, 933-938.
40. C. C. Huang and H. T. Chang, *Chem. Commun.*, 2007, DOI: 10.1039/b615383f, 1215-1217.
41. H. Kawasaki, K. Yoshimura, K. Hamaguchi and R. Arakawa, *Anal. Sci.*, 2011, **27**, 591-596.
42. C. M. Hofmann, J. B. Essner, G. A. Baker and S. N. Baker, *Nanoscale*, 2014, **6**, 5425-5431.

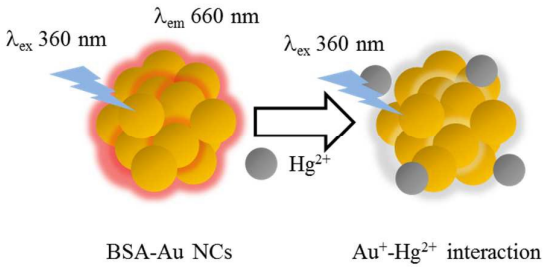

Fluorescence sensing of Hg^{2+} ions by BSA–Au NCs based on the metallophilic interaction between Hg^{2+} and Au^{+} ions